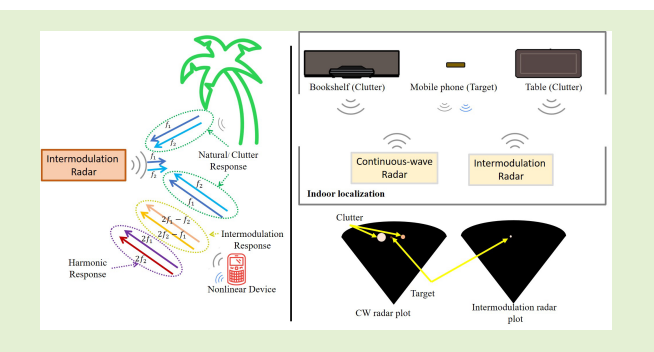


# Utilizing Passive Intermodulation Response of Frequency-Modulated Continuous-Wave Signal for Target Identification and Mapping

Ashish Mishra<sup>®</sup>, Student Member, IEEE, Jing Wang<sup>®</sup>, Student Member, IEEE, Daniel Rodriguez<sup>®</sup>, Graduate Student Member, IEEE, and Changzhi Li<sup>®</sup>, Senior Member, IEEE

Abstract—In this paper, a passive-intermodulation-based tracking system working with a frequency-modulated continuous-wave (FMCW) is proposed for target identification and localization. Signals in the microwave range are chosen to realize ranging purposes for the benefits of small device size, lightweight, and wide available bandwidth. Depending on whether the nonlinear properties of electrical components, such as diodes, transistors, and mixers, are exploited, the tracking systems can be categorized as linear and nonlinear systems. By nature, the linear tracking methods are vulnerable to surrounding clutter, such as furniture, walls, and other objects, since the reflection signals from clutter are of the same nature as the target. In comparison, the nonlinear



detection methods are attractive owning to the fact that the majority of the clutter does not possess nonlinear properties. Hence, the nonlinear detection system does not "see" the linear clutter and only senses the target exhibiting nonlinear responses. Among all the nonlinear technologies, the intermodulation-based tracking and mapping approach has less path loss than the harmonic-based, smaller circuit size than the subharmonic-based, and simpler tag design and fewer signal licenses required than both of its counterparts. Therefore, in this work, the intermodulation-based technology is adopted, and a new nonlinear tracking system is designed to track the distance of the target in a complex indoor scenario crowded with unwanted objects.

Index Terms—Clutter rejection, intermodulation, nonlinear radar, nonlinear tag, ranging.

# I. Introduction

INEAR continuous-wave sensors based on fundamen-Ital frequency responses have been extensively used for measuring range with high precision [1]–[5]. However, these systems have difficulty distinguishing between environmental clutter and the target of interest since the responses of the target and surrounding clutter are of a similar nature [2]. The clutter signal returns can even mask the target response in a clutter-rich environment. To cope with such issues, active tags have been proposed in the literature to generate an additional frequency shift. For example, an active

Manuscript received April 30, 2021; accepted May 24, 2021. Date of publication May 27, 2021; date of current version August 13, 2021. This work was supported by the National Science Foundation (NSF) under Grant ECCS-1808613, Grant ECCS-2028863, and Grant ECCS-2030094. The associate editor coordinating the review of this article and approving it for publication was Dr. Kagan Topalli. (Corresponding author: Ashish Mishra.)

The authors are with the Department of Electrical and Computer Engineering, Texas Tech University, Lubbock, TX 79409 USA (e-mail: ashish.mishra@ttu.edu; changzhi.li@ttu.edu).

Digital Object Identifier 10.1109/JSEN.2021.3084205

backscatter-based sensor operating in the frequency-modulated continuous-wave (FMCW) mode was proposed [6]. The active backscatter tag was mainly composed of a voltage-controlled oscillator (VCO) acting as the signal source and a mixer for up/down conversion. The tracking system transmitted out a signal with a fundamental frequency of  $f_c$ . While the clutter directly reflected back the transmitted signal without any frequency modification, the active backscatter tag captured the signal and the mixer modulated it with the signal from the VCO with frequency  $f_m$ , which is normally at kHz or MHz range. After the frequency conversion process, the generated  $f_c \pm f_m$  tones were transmitted by the tag back to the tracking system. By detecting the additionally generated frequency shift  $f_m$ , the sensors' tag could help the user differentiate the tag from the clutter. However, the tag is active in nature because of the active electronic components used (i.e., oscillator, etc.), which means that they are dependent on the battery/portable power supply for operation. Another drawback is that the freerunning VCO's frequency drifts with time, which may compromise system performance. To overcome this issue, a frequency synthesizer that generates locked and stable signal can be used

1558-1748 © 2021 IEEE. Personal use is permitted, but republication/redistribution requires IEEE permission. See https://www.ieee.org/publications/rights/index.html for more information.

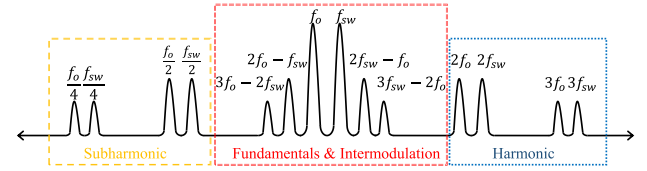


Fig. 1. Nonlinear responses from a typical nonlinear device.

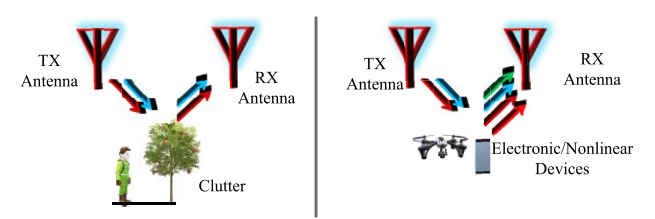


Fig. 2. Responses from clutter and electronic/nonlinear devices.

instead at the tradeoff of increased system cost and larger tag size. In comparison, some nonlinear technologies have alluring advantages for their passive mode operation in tag [7]–[10].

For clutter suppression purposes, some radars transmit two or more frequencies [11]. These signals are transmitted either simultaneously or sequentially. These frequency diversity radars can measure higher ranges with greater detection probability and also limit false alarms. However, these radars suffer from several technical challenges: generation of unwanted intermodulation tones which might affect measurements, and complexity in signal processing [12].

In nonlinear tracking systems, the tag modulates the fundamental tone(s) transmitted by the system using the nonlinear behavior of electrical components, such as diodes, transistors, and mixers. Fig. 1 shows some of the nonlinear responses generated by a typical nonlinear device. By detecting the nonlinear responses generated by the tag, the nonlinear tracking systems can identify and track the tag from surrounding clutter, as shown in Fig. 2. Note that exceptions can occur due to the rusty bolt effect when metal oxide and metal layer make the clutter nonlinear in behavior, causing the clutter to become a source of interference at a high-power level, typically beyond 40 dBm (10 W). [13], [14]

The most common nonlinear sensor is the harmonic sensor. The harmonic tag commonly consists of a frequency multiplier (i.e., diode, transistor) and antenna(s). The receiving antenna captures the fundamental tone f and multiplies it in the frequency multiplier to generate a series of harmonic responses nf at multiples of the fundamental tone, where n = 2, 3, 4, etc. If the transmit signal of the system has a bandwidth of BW, the bandwidth of the harmonic responses will be multiples of BW, i.e., nBW. Generally, for a harmonic system, n is chosen as 2, as typically, the  $2^{nd}$  harmonic response is the strongest response among the rest of the harmonics. The benefit of using a harmonic tracking system is that since the frequency multiplier is passive in nature, the harmonic tag does not require a battery, making the life cycle of the tag immune to the battery limitation. However, because the fundamental frequency is typically in the GHz range, its 2<sup>nd</sup> harmonic is normally located in a different frequency region. The radio-frequency (RF)/microwave spectrum

ranging from MHz to GHz is divided into multiple regions based on their use, such as mobile communication, radio navigation, space communication, etc. Each frequency region has a license associated with it based on the use to avoid one signal from distorting the other. Therefore, harmonic systems require multiple frequency licenses for operation. In addition, as propagation path loss increases with frequency, the harmonic responses suffer from more path loss than the  $f \pm f_m$  tones in the aforementioned active backscatter-based linear tracking system.

Another nonlinear technology is subharmonic [15]. The working principle of the subharmonic sensor is opposite to the harmonic one. The subharmonic tag has a frequency divider, which divides the captured signal frequencies f and bandwidth BW by a factor of n, i.e., the new frequencies and bandwidth are f/n and BW/n. For example, if the transmit frequencies of the system are from 10 GHz to 12 GHz and n is chosen as 2, the subharmonic tag will divide the captured frequencies by a factor of 2, which means the received frequencies of the tracking system will range from 5 GHz to 6 GHz. Thus, the received signal bandwidth becomes half, i.e., 1 GHz, which may affect the range resolution of the system if it is operating in the FMCW mode. Compared with the harmonic system that operates at the same fundamental frequency(s), the subharmonic sensor has lower path loss due to the lower nonlinear frequency(s), yet comes at the cost of a larger receiver and tag size. In addition, since the frequency divider is a type of active components, the subharmonic tag requires a continuous power supply to operate. As a result, it cannot be sealed to reduce wear and tear. Furthermore, it also requires multiple frequency licenses, which increases the overall implementation cost.

There has been research going on towards exploiting the intermodulation behavior exhibited by passive nonlinear devices to differentiate the target of interest from the clutter [16]. The mathematical model shown by the Volterra series and time-domain analysis is discussed in [17], [18]. According to the intermodulation theory, intermodulation products occur when the input to the nonlinear device is composed of two or more frequencies. For example, assuming two fundamental tones  $f_o$  and  $f_{sw}$  transmit towards a nonlinear device, except generating the aforementioned harmonic responses, additional frequency products at the sum and difference frequencies of the fundamental frequencies and at sum and difference of multiples of those frequencies will also be created, which can be represented as  $pf_o \pm qf_{sw}$ , where p and q are integers. The order of these intermodulation products is the sum of p and q. In many scenarios, the  $3^{rd}$  order intermodulation products (IMP3s), i.e.,  $f_{IMI} = 2f_o - f_{sw}$ and  $f_{IMh} = 2f_{sw} - f_o$ , are of primary interest because they are in the closest vicinity to the two fundamental tones. Furthermore, since the two IMP3s are identical in power level and are of the same vicinity to the fundamental tones, only one IMP3 is selected and discussed in the following analysis, which is the lower IMP3 (i.e.,  $f_{IMl}$ ). If one of the fundamental tones has a frequency sweep or both of the fundamental frequencies sweep, there will be one bandwidth in the transmit signal or two separate bandwidths, respectively.

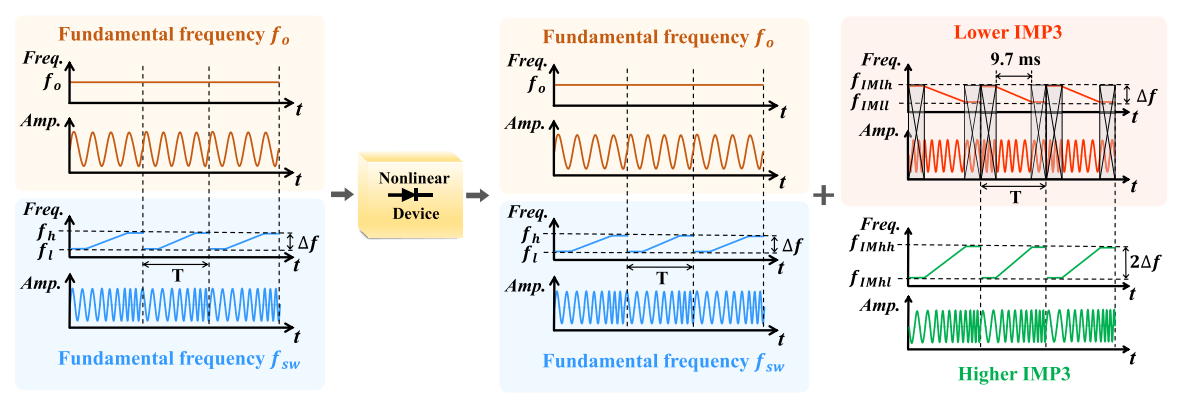


Fig. 3. Fundamental frequencies and corresponding intermodulation and fundamental responses from a nonlinear tag.

f <sub>o</sub> sweeps	f <sub>sw</sub> sweeps	$f_{IMl}$	$f_{IMh}$	IMP3
BW	0	2 BW	BW	3 <i>BW</i>
$BW/2^*$	$BW/2^*$	1.5 <i>BW</i>	1.5 <i>BW</i>	3 <i>BW</i>
0	BW	BW	2 <i>BW</i>	3 <i>BW</i>

\*Sweep is in opposite direction

The bandwidth of the IMP3 remains the same i.e. 3BW, however, the lower IMP3 varies depending on the number of tones swept, which is summarized in Table I.

The conditions discussed in Table I hold true when fundamental tones do not crossover ( $f_o < f_{sw}$ ). For example, consider the situation where the two fundamental tones are  $f_o = 5.8$  GHz and  $f_{sw} = 5.9$ GHz, after passing through a nonlinear device, the lower IMP3 of 5.7 GHz will be created. If  $f_o$  sweeps from 5.8 GHz to 5.85 GHz and  $f_{sw}$  remains constant, the resulting lower IMP3 will range from 5.7 GHz to 5.8 GHz. The bandwidth of the lower IMP3 is 100 MHz, which is two times the bandwidth of the fundamental tones. For the condition when  $f_{sw}$  sweeps from 5.9 GHz to 5.95 GHz while  $f_0$  remains constant at 5.8 GHz, the resultant lower IMP3 sweeps from 5.65 GHz to 5.7 GHz. In this scenario, the bandwidth of the desired IMP3 is the same as the fundamental. For the situation when  $f_o$  sweeps from 5.8 GHz to 5.7 GHz and  $f_{sw}$  sweeps from 5.9 GHz to 6 GHz, the lower IMP3 response ranges from 5.4 GHz to 5.7 GHz. Now the bandwidth is 1.5 times the bandwidth of the fundamental tones. Hence, the intermodulation tracking system has a flexible bandwidth depending on the situation or requirements of the intended applications.

Though the intermodulation sensor has higher propagation path loss than the subharmonic sensor for its higher nonlinear frequency, it comes at the benefit of relieving the licensing issue, as the fundamental and IMP3s lie in the same licensed frequency region. In addition, since the harmonic and subharmonic responses are widely separated in the frequency region compared to the fundamental tone(s), the tag of these tracking systems requires either two different antennas or a single antenna operating at two frequency regions. The same is also true for the matching circuit in these tags. Advantageously, only one antenna and one matching circuit need to be designed to operate at a single frequency region for the intermodulation tag, making the tag structure simpler and smaller than the corresponding harmonic and subharmonic ones.

The above discussions can be summarized as that the intermodulation-based microwave sensor resolves the issue faced by fundamental-response-based microwave sensors such as clutter rejection. The proposed sensor also solves the drawback of the licensing issue, has lower path loss than the harmonic, has a smaller tag/receiver size compared to the subharmonic-based microwave sensor, and requires a passive tag instead of an active one.

This paper discusses the use of passive intermodulation response to distinguish and track the target of interest in the presence of environmental clutter. Potential applications include search and rescue, target identification and tracking, and security monitoring. In [19], the concept and feasibility of utilizing intermodulation response for target motion discrimination were verified. The work was expanded in [16] to measure human vital signs in the presence of background noises. The radar discussed in [16] was operated in Doppler mode and hence can be used for determining the motion frequency of the target and cannot be used for ranging applications. After that, the frequency shift keying (FSK) mode was introduced in [20] for ranging purposes based on the vital signs of the human target. However, the FSK mode can only localize a moving target based on the Doppler effects. To locate both moving and stationary targets and thus achieve ubiquitous sensing in a realistic, complex indoor environment, an FMCW mode is devised for passive intermodulation. In this mode, the probing frequency for localization is modulated by the targeted nonlinear device. In [20], part of the fundamental tones was absorbed in the transmitting path after the quadrature hybrid before being transmitted out. In this work, there is no power loss in the transmitter apart from the 3 dB loss at the quadrature hybrid, which significantly increases the sensor's detection range since the power level of the transmitted tones is critical for ranging sensitivity.

The paper is divided into five sections. Section II explains the fundamental theory. Section III discusses the design of the FMCW tracking device. The range detection and 2-D map measurements are presented in Section IV. Finally, conclusions are drawn in Section V.

# II. THEORY

When two frequencies  $f_o$  and  $f_{sw}$  are passed through a nonlinear device, additional intermodulation tones  $pf_o \pm qf_{sw}$ , where p and q are integers, are generated. Since most of the

natural clutter does not generate intermodulation frequencies, they can be distinguished from the target by examining the responses at the intermodulation tones. Theoretically, the 5<sup>th</sup> order and higher intermodulation tones can also be utilized. However, since IMP3s typically have the largest power level and are the closest to the fundamental tones among the rest of the intermodulation products in the same licensed frequency region, only the IMP3s (i.e.,  $f_{IMI} = 2f_o - f_{sw}$  and  $f_{IMh} = 2f_{sw} - f_o$ ) are of interest in the proposed system. Furthermore, since the two IMP3s are identical in power level and are of the same vicinity to the fundamental tones, only one IMP3 is selected and discussed in the following analysis, which is the lower IMP3 (i.e.,  $f_{IMI} = 2f_o - f_{sw}$ ).

As shown in Fig. 3, in the proposed FMCW system,  $f_0$  is kept constant, while  $f_{sw}$  sweeps from  $f_l$  to  $f_h$  to generate a bandwidth  $BW = f_h - f_l$  required for ranging purposes. Note that the frequency sweep has a step size  $f_{step}$  of 10.1 MHz. Conventional processing of the stepped-frequency-continuous wave mode requires two channels (i.e., in-phase and quadrature channels) [21]. In this work, the stepped signal was approximated as a linear ramp signal since processing the ramp signal requires only one channel. The range offset caused by the discrete frequency step was accounted for and calibrated out in the range calculation stage. The frequency sweeping is controlled by a chirp signal with a chirp repetition rate of 1/T, which has a typical range of hundreds of Hertz. The slope of the chirp signal is represented as  $\gamma = BW/T$ . The transmit signal for a single chirp can be expressed as

$$T(t) = e^{j(2\pi f_o t + \phi)} + e^{j(2\pi f_{sw} t + \pi \gamma t^2 + \phi)}$$
(1)

where  $\phi$  is the initial phase. A nonlinear device is used to generate the IMP3s and the  $f_{IMh}$  is suppressed by bandpass filters (BPF). Details will be provided in the next section. The formed LO signal is

$$L(t) = e^{j(2\pi f_{IMl}t - \pi \gamma t^2 + \phi + \phi_{d,LO})}$$
 (2)

where  $\phi_{d,LO}$  accounts for the phase delay caused by the isolator, circulator, nonlinear device, filter, and amplifier in the LO path. As shown in Fig. 4, the tag incepts the transmitted fundamental tones, generates a second pair of IMP3s, and retransmits them back to the FMCW sensor with a round-trip-time-of-flight of  $\tau = \frac{2D}{c}$ , where D is the distance to the tag. Since the chirp repetition rate is normally much faster compared to the target motion change, D can be assumed to be constant for each chirp window. The received signal at the sensor receiver can be written as

$$R(t) = \sigma L \left( t - \tau - \phi_{d,T} \right) \tag{3}$$

where  $\sigma$  is the amplitude of the received signal normalized to the LO signal and  $\phi_{d,T}$  represents the phase delay due to the conversion of fundamental tones to the IMP3s in the tag. After mixing the  $f_{IMI}$  in the LO path with the  $f_{IMI}$  signal at the mixer, the resulting baseband signal can be mathematically expressed as

$$B(t) = L(t) \times R^*(t) = \sigma e^{j(f_b t + p_b + \Delta \phi)}$$
(4)

where  $\Delta \phi$  is the residual phase,  $p_b$  is the slow-time phase history, and  $f_b$  is the true beat frequency, which is proportional

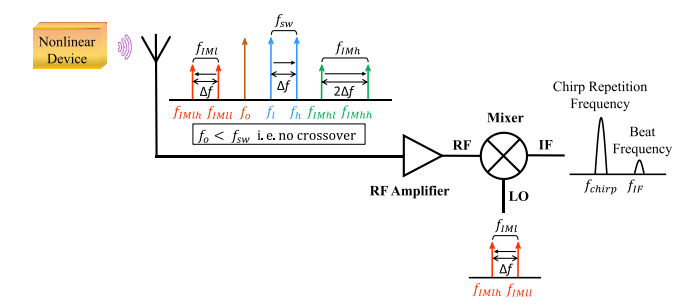


Fig. 4. Frequencies present in baseband signal.

to the distance to the tag. In a linear-frequency-changing microwave sensor, a delay will shift the echo (received) signal in time. This causes a difference in the received and transmitted frequency, which is called the beat frequency. However, there is an additional frequency shift  $f_{offset}$  due to  $\Delta\phi$  over the chirp duration. The measured beat frequency  $f_{b,m}$  can be expressed as

$$f_{b,m} = f_b + f_{offset} = \frac{2\gamma D}{c} + f_{offset}$$
 (5)

where c is the speed of light. The target range can be derived from Equation (5) as

$$D_m = D + D_{offset} = \frac{cf_b}{2\gamma} + D_{offset} \tag{6}$$

where  $D_{offset}$  is the range offset associated with  $f_{offset}$ . Hence, one-time calibration is needed to account for  $D_{offset}$ .

$$D = D_0 + \Delta D_{Doppler} + mD_u \tag{7}$$

where  $D_0$  is the true target location, m is a natural number and  $D_u = \frac{c}{2f_{step}} = 14.8$  m is the maximum unambiguous range for  $f_{step} = 10.1$  MHz. Since the target is stationary (i.e., v = 0),  $\Delta D_{Doppler} = \frac{f_{IMI}}{BW}v\tau = 0$ , where  $\tau$  is the sweep time of the chirp. As shown in [22], the recovered time/range equation is a periodic signal that repeats every time the maximum unambiguous range is reached. Therefore, for any value of m, the same range will be obtained.

The FMCW sensor can detect multiple targets because it possesses a frequency bandwidth BW. The ability to distinguish two closely spaced targets is referred to as range resolution, which is inversely proportional to the bandwidth and is calculated as

$$\Delta D = \frac{c}{2RW} \tag{8}$$

#### III. DESIGN

#### A. Transmitter and LO Path Design

Fig. 5 shows the block diagram of the proposed passive-intermodulation-based FMCW system. The components used in the system are shown in Fig. 6.  $f_o = 5.79$  GHz is generated by a signal generator SG 1 and a frequency sweep  $f_{sw}$  from  $f_l = 5.85$  GHz to  $f_h = 6.05$  GHz at a sweeping rate of around 12 Hz is generated by SG 2. The control signal of the frequency sweep in SG 2 is a chirp signal, and it is used as the synchronization signal for data processing. Thus, it is connected to the data acquisition device (NI-DAQ-6009). Typically, the chirp repetition rate is in the hundreds of Hertz

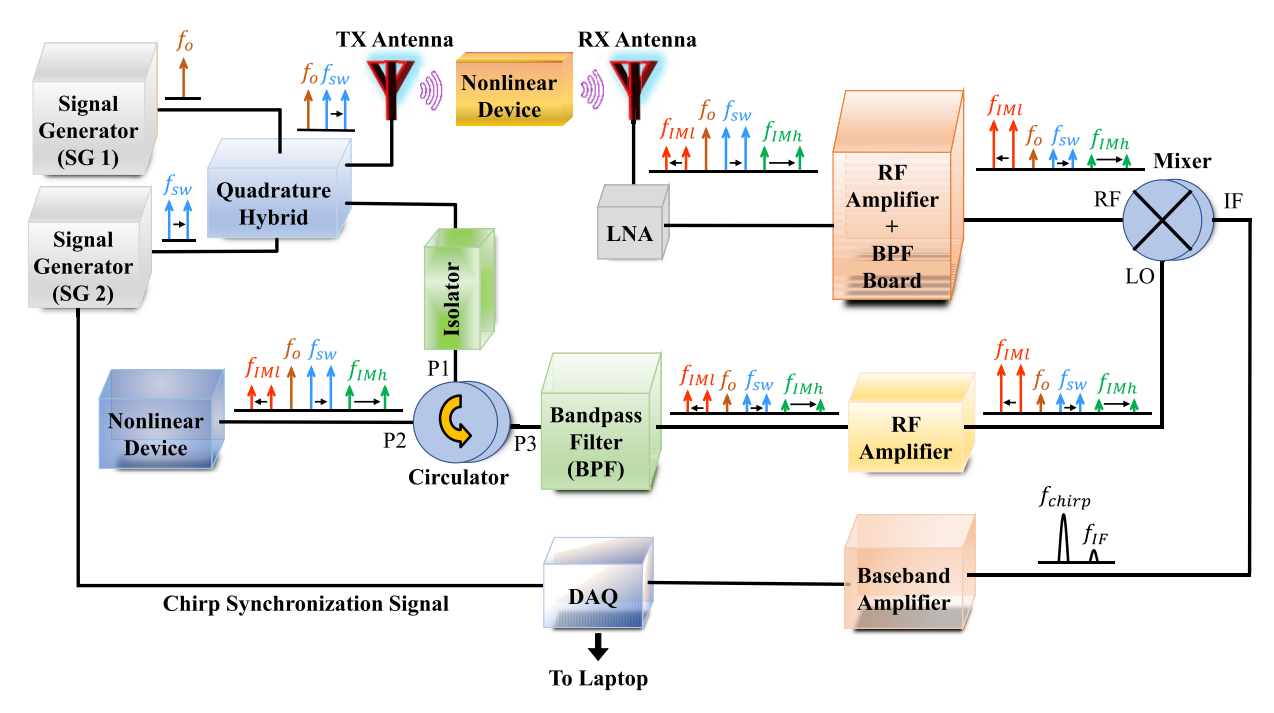


Fig. 5. Block diagram of intermodulation radar operating in C-band.

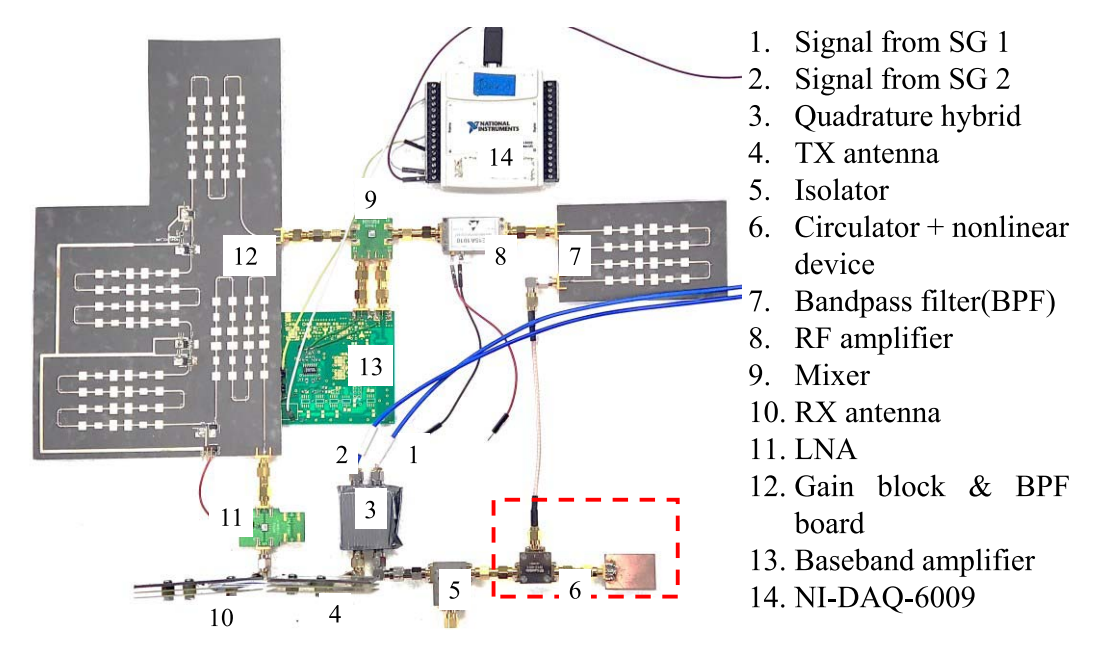


Fig. 6. Hardware prototype of the intermodulation based FMCW radar.

range for moving target tracking and localization applications. The chirp repetition rate of the signal generator was 12 Hz. The chirp repetition rate determines the maximum Doppler shift that the radar can measure. The 12 Hz chirp repetition rate can only measure Doppler frequency of up to 6 Hz and hence cannot be used for measuring the walking speed of humans, which produces more than 30 Hz Doppler shift at a walking speed of 1m/s.

The focus of the work was general target localization and mapping in a clutter-rich environment. It should be noted that for a moving target or a human subject with breathing/heartbeat, identifying the target would benefit from other signal processing-based clutter removal techniques [23]–[29].

The range and Doppler for a moving target can be estimated with this radar by utilizing the following method. The range can be estimated by first performing FFT over chirp to obtain the beat frequency, which determines the range information. Two methods can further estimate the vital signs information. In the first method, the range is calculated for each chirp. After getting the range information, an FFT is performed over the range bin for multiple chirps to estimate the change of range over time to obtain the vital signs information. In the second method, the baseband signal is arranged as a function of the transmitted frequency signal, as shown in Table II.  $C_{X,Y}$  in Table II represents the baseband value corresponding to the  $X^{th}$  chirp and Y transmitted frequency. FFT can be performed

TABLE II
OBTAINING MOTION FREQUENCY FROM MULTIPLE CHIRPS

Chirp	$f_{sw}$	$f_{sw} + \Delta f$		$f_{sw} + (N-1)\Delta f$
1	C <sub>1,1</sub>	C <sub>1,2</sub>	_	$C_{1,N}$
2	$C_{2,1}$	$C_{2,2}$	_	$C_{2,N}$
I				1
M - 1	$C_{M-1.1}$	$C_{M-1.2}$	_	$C_{M-1.N}$
М	$C_{M,1}$	$C_{M,2}$	_	$C_{M,N}$

by selecting a column corresponding to a particular transmitted frequency. Please note that in both methods, the chirp repetition rate determines the sampling frequency. The limited chirp repetition rate limits the maximum motion frequency that the radar can measure.

Because the free-running VCOs cannot be used to maintain coherence as they suffer from frequency drift and the drift can be different for the three signal generators, in [14], [17], frequency synthesizers were used to maintain the coherence between the fundamentals and LO frequencies by sharing the same reference between the three signal generators. In the new architecture, since the same transmit frequencies are used for the LO frequencies, the correlation between the LO and fundamental tones is maintained without the need for any reference signal, which helps in avoiding the use of expensive frequency synthesizers and reducing the cost and size.

10 dBm of fundamental tones are generated by SG 1 and SG 2, respectively, and sent to a quadrature hybrid, which equally distributes the signal along two paths. One path with 7 dBm power for each tone is connected to the TX antenna for signal transmission. The other path with the same amount of power is passed to the LO port of the mixer for the down-conversion of the received signal.

In the LO path, a circulator is used to direct the signal from the quadrature hybrid to a nonlinear device (i.e., a diode) to generate the IMP3s, which along with the fundamental tones, are further directed to the bandpass filter. An isolator is connected after the quadrature hybrid and before the circulator to prevent the RF reflections from the rest of the LO path from leaking back to the TX antenna. The bandpass filter is designed to attenuate the fundamental and  $f_{IMh}$  tones by 30 dB so that the undesired tones do not have sufficient power to drive the mixer. Next, the output of the bandpass filter is passed to an RF amplifier to amplify the desired  $f_{IMl}$  frequencies by 40 dB, resulting in a LO power level of 10 dBm.

#### B. Nonlinear Tag

The gain of the TX antenna is 14 dB. The tag has an antenna array with a gain of 19 dB. As per the free-space path loss model, the path loss for 5.8 GHz carrier frequency at a distance of 1 m is approximately 15 dB. Therefore, the tag captures around -8 dBm power level of fundamental tones at a 1 m distance. According to the measurement data [16], the conversion loss of the tag lies between 22 dB to 28 dB for input power levels ranging from -10 dBm to 0 dBm. Therefore,

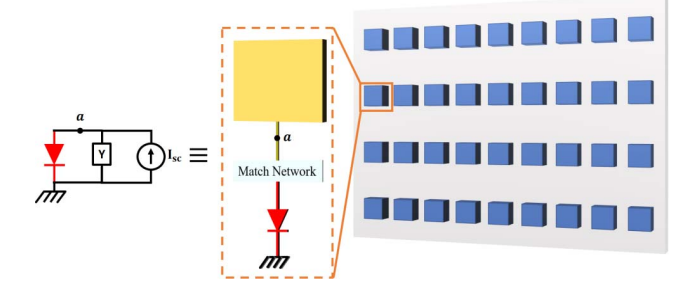


Fig. 7. Nonlinear tag with a nonlinearly loaded antenna and its equivalent circuit in inset.

for an incident power level of -8 dBm, -31 dBm of IMP3s will be generated due to conversion loss, which is backscattered towards the RX antenna. Similarly, the RX antenna has an approximate gain of 14 dB. Hence, the path loss will be almost equal for the backscattered response from the tag to the sensor as the transmitted tones from the sensor to the tag since the frequencies are very close to one another.

The passive nonlinear tag was designed on RT/Duroid 5880 substrate using Infineon's BAT 15-03W diode. A simple matching network was designed using stubs to match the diode input port with the antenna's input port (i.e.,  $50\Omega$ ). Fig. 7 shows the equivalent model of a nonlinearly loaded antenna. The TX antenna sends out a radiation pattern at  $f_o$  and  $f_{sw}$  frequency tones containing E-field information denoted as  $E_i$ , which is the summation of the E-fields of each individual tone along the broadside direction. Here,  $I_{sc}$  is the short circuit current generated due to  $E_i$  and Y is the linear admittance. The final tag was implemented using  $9 \times 4$  arrays of the unit cells as shown in Fig. 7. The simulation results of the Spice model at the  $3^{rd}$  order response are as shown in [16].

#### C. Receiver Design

A 15 dB path loss will be experienced by the IMP3s again on their trip back. Hence, they are received by the RX antenna (14 dB gain) with a power level of -46 dBm. A low noise amplifier (LNA) amplifies the received signal by approximately 15 dB, which is connected to a series of bandpass filters and gain blocks. The bandpass filters and gain blocks board provides an attenuation of 50 dB to the fundamental and  $f_{IMh}$  tones and a gain of 20 dB to the  $f_{IMl}$  tones.

The current system was compared to the existing state of the art, as shown in Table III. Due to the limited transmitting power and antenna gain for the radar, the intended applications are indoor localization. In this work, the S-parameter model of the diode was used for designing the matching circuit, and the Spice model of the device was used for measuring the conversion loss of the tag. The X-parameter measurement of the tag would provide a better understanding of the nonlinear behavior of the tag [33]. It was not used in this work due to the absence of X-parameter measurement equipment.

#### IV. MEASUREMENTS

## A. Calibration

Through extensive experimentation, it was revealed that the phase delays introduced by electronic components, such as

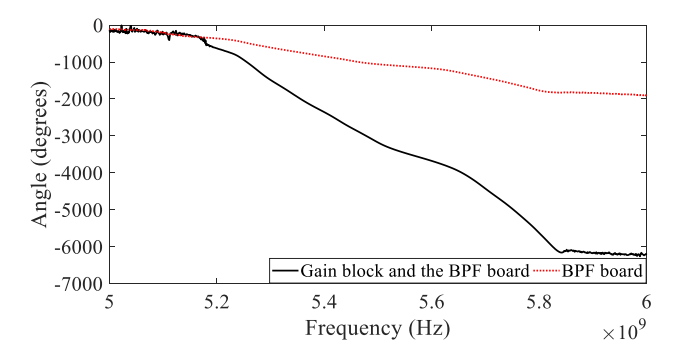


Fig. 8. Phase response of the gain block and bandpass filter and BPF boards.

TABLE III

COMPARISON OF THE CURRENT WORK WITH THE EXISTING

NONLINEAR RADARS

Works	Transmit Power	Radar antenna gain	Tag type
[30]	65 dBm	> 38 dBi	Passive
[31]	30 dBm	40 dBi	Active
[32]	40 dBm	50 dBi	Passive
This work	7 dBm	15 dBi	Passive

diodes, bandpass filters, gain blocks, isolator, etc., could form a large phase shift in the signal chain and cause a large range offset in the measurements. In addition, the conversion of the fundamental tones to the IMP3 responses in the target also results in phase delay. Therefore, a calibration procedure is required to obtain the range offset.

A one-time calibration was performed by placing the tag in front of the tracking system at 0.6 m away. The  $D_m$  was calculated as 16.2 m using Equation (6).

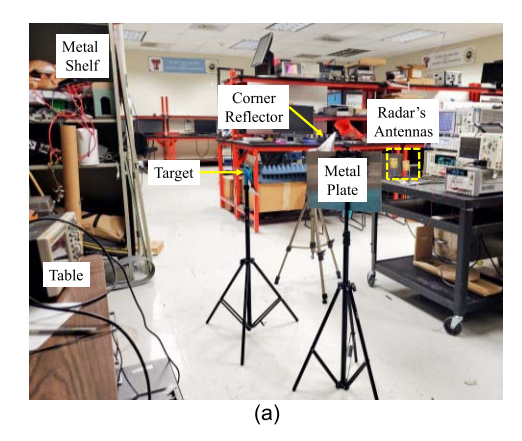
Substituting Equation (7) into Equation (6), setting m as 1, and assuming v = 0, the measured range can be derived as  $D_m = D_0 + D_u + D_{offset}$ .

The group delay  $\tau_g$  of the components can be calculated using the formula

$$\tau_g = -\frac{d\phi_{rad}}{d\omega} = -\frac{d\phi_{deg}}{df \times 360} \tag{9}$$

here  $\phi_{rad}$  is the phase in radians,  $\phi_{deg}$  is the phase in degrees, and  $\omega$  is in radians /sec, and f is in Hertz.

Fig. 8 shows the phase delay measured by the vector network analyzer (NI-PXIe 5630). For 5.7 GHz, the phase delay due to the BPF board in the LO path was measured as 1425° using a vector network analyzer. Similarly, the phase delay introduced by the gain block and the BPF board in the receiver path was measured 4427°. The conversion process occurs in the LO and the receiving paths (i.e., NL device and target). Each conversion of fundamental tones to IMP3s generates a phase change of 180° as per the Volterra equation, where the 3<sup>rd</sup> order term is negative [34]. The components in the LO path provide a negative range offset while the components in the receiving path provide a positive range offset. Therefore, the net phase delay was calculated as 3002° (i.e., 5150°+180°-790°-180°). This corresponds to a range offset of 0.44 m. The remaining range offset of 0.36 m (16.2 m -14.8 m -0.6 m - 0.44 m) was assumed to be introduced by other RF components (cables, LNA, circulator, etc.). Hence,  $D_{offset}$ 



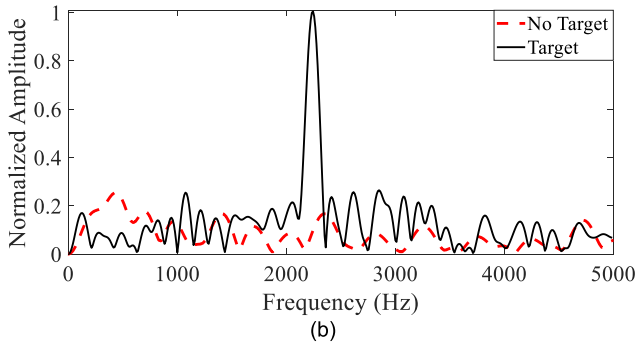


Fig. 9. (a) Experiment setup; (b) Frequency spectrum when the target was at 0.6 m and when the target was removed with antennas pointing at  $90^{\circ}$ 

was equal to 0.8 m. The detailed signal processing will be explained in the following section.

### B. Range Measurement

The experimental setup is shown in Fig. 9(a). The tag was the target, and it was intentionally surrounded by unwanted objects (i.e., corner reflector, metal plate, and metal shelf) to mimic a realistic indoor localization scenario. The baseband and chirp data were recorded using the NI-DAO-6009 with a sampling frequency of 10 kHz. Baseband data corresponding to the chirp region was identified and selected based on the synchronization chirp signal. Fast Fourier transform (FFT) was performed on the baseband data to obtain the beat frequency for each chirp window. Fig. 9(b) shows the frequency spectrum plots obtained when the target was 0.6 m in front of the tracking system and when the target was removed. A beat frequency of 2224 Hz can be identified on the frequency spectrum plot when the target was present, while no clear frequency peak shows up on the spectrum in the absence of the target because the clutter does not generate nonlinear responses.

More measurements were performed from 0.6 m to 1.9 m with a step size of 0.1 m. Fig. 10 shows the beat frequencies obtained when the target was at 0.6 m, 1.2 m, and 1.8 m, respectively. The measured data versus the ground truth plot is shown in Fig. 11. Note that the range offsets  $(D_{offset}, D_u)$  measured in the calibration stage was subtracted from all the measurements.

# C. Target Mapping

The performance of the proposed passive-intermodulationbased FMCW sensor is compared with a conventional state

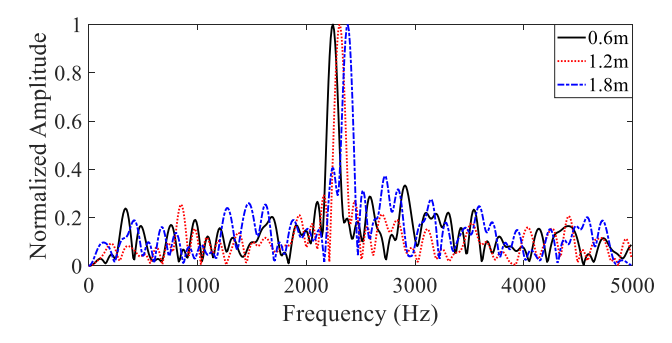


Fig. 10. Frequency spectrum when the target was at 0.6 m, 1.2 m, and 1.8 m, respectively.

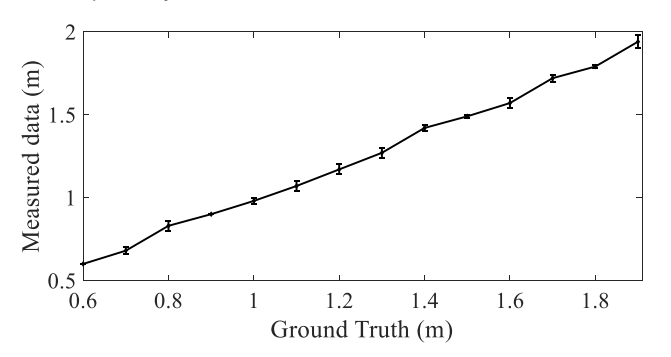


Fig. 11. Distance recorded by the proposed radar sensor and error analysis.

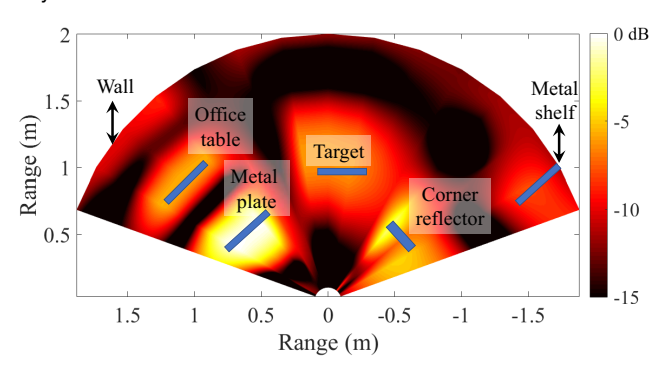


Fig. 12. Target mapping using a conventional FMCW sensor.

of the art FMCW microwave sensor, which is designed to operate approximately in the same frequency region, have a larger bandwidth of 320 MHz, and equip with the same sets of TX/RX antenna. The FMCW sensor had a chirp repetition rate of 350 Hz. The same environmental setup as the range measurement scenario was used, except that the target was located at 1 m distance this time.

The antennas of the FMCW sensor were steered to cover the angle region from 20° to 160° with a step size of 10°. As shown in Fig. 12, both the target and the clutter were detected by the FMCW sensor because all of them reflect the fundamental tones. The illumination level depends on the radar cross-section (RCS), which is related to the object material, size, incidence angle, etc. RCS is the estimate of a target's ability to reflect radio-frequency signals in the direction of the microwave receiver. It is the ratio of the backscatter power per steradian in the direction of the sensor (from the target) to the power density that is captured by the target [35]. A change in the incident angle can change the reflected signal

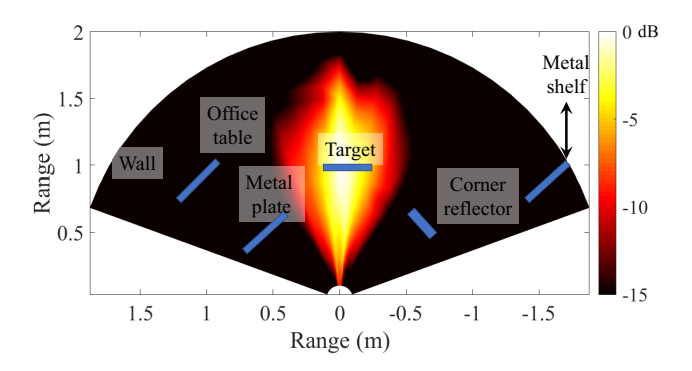


Fig. 13. Target mapping using the proposed intermodulation based FMCW sensor.

strength as discussed in [36]. Therefore, the RCS of the targets is dependent on the incident angle. The maximum RCS value of a flat metal plate is obtained when the incident angle is 0°. The maximum RCS of the corner reflector is calculated as 5.1  $m^2$  using the equation  $\frac{4\pi L^4}{3\lambda^2}$ . L is the distance between the apex and base of the corner reflector, which is 24 cm. Note that a trihedral corner reflector has a relatively uniform response for a small variation of incident angle.

Due to the rectangular geometry  $(26.7 \text{ cm} \times 19.6 \text{ cm})$  and the metal sheet  $(30.5 \text{ cm} \times 22.9 \text{ cm})$ , the maximum RCS for both of them is calculated using  $\frac{4\pi H^2 W^2}{12}$ , where H and W are the corresponding dimensions. The RCS is calculated as 12.9  $m^2$  for the tag and 22.7  $m^2$ for the metal plate. The metal shelf has a complex shape and the dimensions for the RCS are difficult to define. As a result, the maximum RCS of the metal shelf is not calculated. Nonetheless, based on its large physical size  $(1.8 m \times 2.4 m)$ and the metal body, its maximum RCS should be much larger than the tag, metal sheet, and corner reflector. An office table  $(0.8 m \times 1.2 m)$  was also present in the measurement environment. Fig. 9(a) shows the measurement setup, and the objects present in the vicinity.

When the intermodulation based FMCW sensor was used to sense the same environment, the sensor was steered to cover the region from 20° to 160° similar to the previous case. Fig. 13 shows the final result of the target 2-D map using the intermodulation based FMCW sensor. It can be seen that only the target was detected when the intermodulation based FMCW sensor was used. Note that the reason why the target illumination spreads out in the radial direction is that the range resolution is 0.75 m according to Equation 8. An increase in bandwidth can lower the range resolution and reduce the radial fan out. The spread in the tangential direction is caused by the antennas' large half-power beamwidth (HPBW), which is 40°. This can be improved if antennas with smaller HPBW are adopted. The capability and applications of this sensor can also be enhanced by utilizing phase arrays antennas and MIMO techniques.

### V. CONCLUSION

A passive intermodulation tracking system operating in FMCW mode was successfully designed and measurements were recorded. The tag was able to generate a passive intermodulation response and the sensor was able to successfully

differentiate and localize the tag in a typical lab environment with various clutter. Hence, it has the potential to be successfully implemented in indoor target identification and localization. Compared to the other nonlinear tracking system types, the proposed technology operates in one licensed frequency region for transmitting and receiving signals. This simplifies the hardware design and avoids the licensing issue due to multi-region operation. The tag is passive in nature. Thus, its lifetime is limited by wear and tear alone. The future work is to make the system portable in order to expand the applications for this sensor.

#### REFERENCES

- S. Scherr et al., "Influence of radar targets on the accuracy of FMCW radar distance measurements," *IEEE Trans. Microw. Theory Techn.*, vol. 65, no. 10, pp. 3640–3647, Oct. 2017.
- [2] G. Wang, C. Gu, T. Inoue, and C. Li, "A hybrid FMCW-interferometry radar for indoor precise positioning and versatile life activity monitoring," *IEEE Trans. Microw. Theory Techn.*, vol. 62, no. 11, pp. 2812–2822, Nov. 2014.
- [3] M. Mercuri et al., "Vital-sign monitoring and spatial tracking of multiple people using a contactless tracking system-based sensor," Nature Electron., vol. 2, pp. 252–262, Jun. 2019.
- [4] G. Charvat, A. Temme, M. Feigin, and R. Raskar, "Time-of-flight microwave camera," Sci. Rep., vol. 5, Oct. 2015, Art. no. 14709.
- [5] R. Komissarov *et al.*, "Partially coherent radar unties range resolution from bandwidth limitations," *Nature Commun.*, vol. 10, no. 1, p. 1423, Mar. 2019. [Online]. Available: https://www.nature.com/articles/s41467-019-09380-x, doi: 10.1038/s41467-019-09380-x.
- [6] M. Sadegh Dadash, J. Hasch, P. Chevalier, A. Cathelin, N. Cahoon, and S. P. Voinigescu, "Design of low-power active tags for operation with 77–81-GHz FMCW radar," *IEEE Trans. Microw. Theory Techn.*, vol. 65, no. 12, pp. 5377–5388, Dec. 2017.
- [7] K. A. Gallager, "Harmonic tracking system: Theory and applications to nonlinear target detection, tracking, imaging and classification," Ph.D. dissertation, Dept. Elect. Eng., Pennsylvania State Univ., State College, PA, USA, Dec. 2015.
- [8] T. Berger and S.-E. Hamran, "Harmonic synthetic aperture radar processing," *IEEE Geosci. Remote Sens. Lett.*, vol. 12, no. 10, pp. 2066–2069, Oct. 2015.
- [9] N. Tahir and G. Brooker, "Toward the development of millimeter wave harmonic sensors for tracking small insects," *IEEE Sensors J.*, vol. 15, no. 10, pp. 5669–5676, Oct. 2015.
- [10] A. Singh and V. M. Lubecke, "Respiratory monitoring and clutter rejection using a CW Doppler radar with passive RF tags," *IEEE Sensors J.*, vol. 12, no. 3, pp. 558–565, Mar. 2012.
- [11] I. M. Skolnik, Introduction to Radar Systems, 2nd ed. New York, NY, USA: McGraw-Hill, 1980.
- [12] W. Wang, "Overview of frequency diverse array in radar and navigation applications," *IET Radar, Sonar Navigat.*, vol. 10, no. 6, pp. 1001–1012, Jul. 2016.
- [13] A. W. D. Watson, "Improvements in the suppression of external nonlinearities ('rusty bolt' effects) which affect naval radio systems," in *Proc. IEEE Int. Symp. Electromagn. Compat.*, Aug. 1983, pp. 1–4.
- [14] P. L. Lui, "Passive intermodulation interference in communication systems," *Electron. Commun. Eng. J.*, vol. 2, no. 3, pp. 109–118, Jun. 1990.
- [15] N. El Agroudy, M. El-Shennawy, N. Joram, and F. Ellinger, "Design of a 24 GHz FMCW radar system based on sub-harmonic generation," *IET Radar, Sonar Navigat.*, vol. 12, no. 9, pp. 1052–1057, Sep. 2018.
- [16] A. Mishra and C. Li, "A low power 5.8-GHz ISM-band intermodulation radar system for target motion discrimination," *IEEE Sensors J.*, vol. 19, no. 20, pp. 9206–9214, Oct. 2019.
- [17] J. Landt, E. Miller, and F. Deadrick, "Time domain modeling of nonlinear loads," *IEEE Trans. Antennas Propag.*, vol. AP-31, no. 1, pp. 121–126, Jan. 1983.
- [18] T. Sarkar and D. Weiner, "Scattering analysis of nonlinearly loaded antennas," *IEEE Trans. Antennas Propag.*, vol. AP-24, no. 2, pp. 125–131, Mar. 1976.
- [19] A. Mishra and C. Li, "5.8-GHz ISM band intermodulation radar for high-sensitivity motion-sensing applications," in *Proc. IEEE Radio Wireless Symp. (RWS)*, Jan. 2018, pp. 4–6.

- [20] A. Mishra, W. McDonnell, J. Wang, D. Rodriguez, and C. Li, "Intermodulation-based nonlinear smart health sensing of human vital signs and location," *IEEE Access*, vol. 7, pp. 158284–158295, 2019.
- [21] M. Mercuri, D. Schreurs, and P. Leroux, "SFCW microwave radar for in-door fall detection," in *Proc. IEEE Topical Conf. Bio*med. Wireless Technol., Netw., Sens. Syst. (BioWireleSS), Jan. 2012, pp. 53–56.
- [22] M. Pieraccini, L. Miccinesi, and N. Rojhani, "A Doppler range compensation for step-frequency continuous-wave radar for detecting small UAV," Sensors, vol. 19, no. 6, p. 1331, Mar. 2019.
- [23] D. Zhao, J. Wang, G. Chen, J. Wang, and S. Guo, "Clutter cancellation based on frequency domain analysis in passive bistatic radar," *IEEE Access*, vol. 8, pp. 43956–43964, 2020.
- [24] Z. Peng *et al.*, "A portable FMCW interferometry radar with programmable low-IF architecture for localization, ISAR imaging, and vital sign tracking," *IEEE Trans. Microw. Theory Techn.*, vol. 65, no. 4, pp. 1334–1344, Apr. 2017.
- [25] A. G. Varovoy, L. P. Ligthart, J. Matuzas, and B. Levitas, "UWB radar for human being detection," *IEEE Aerosp. Electron. Syst. Mag.*, vol. 21, no. 3, pp. 10–14, Mar. 2006.
- [26] B.-H. Lee, S. Lee, Y.-J. Yoon, K.-M. Park, and S.-C. Kim, "Adaptive clutter suppression algorithm for human detection using IR-UWB radar," in *Proc. IEEE Sensors*, Oct. 2017, pp. 1–3.
- [27] Z. Peng, L. Ran, and C. Li, "A K-band portable FMCW radar with beamforming array for short-range localization and vital-Doppler targets discrimination," *IEEE Trans. Microw. Theory Techn.*, vol. 65, no. 9, pp. 3443–3452, Sep. 2017.
- [28] C. Will, P. Vaishnav, A. Chakraborty, and A. Santra, "Human target detection, tracking, and classification using 24-GHz FMCW radar," *IEEE Sensors J.*, vol. 19, no. 17, pp. 7283–7299, Sep. 2019.
- [29] A. Lazaro, D. Girbau, and R. Villarino, "Techniques for clutter suppression in the presence of body movements during the detection of respiratory activity through UWB radars," *Sensors*, vol. 14, no. 2, pp. 2595–2618, Feb. 2014.
- [30] Z.-M. Tsai et al., "A high-range-accuracy and high-sensitivity harmonic radar using pulse pseudorandom code for bee searching," *IEEE Trans. Microw. Theory Techn.*, vol. 61, no. 1, pp. 666–675, Jan. 2013.
- [31] N. Tahir and G. Brooker, "Recent developments and recommendations for improving harmonic radar tracking systems," in *Proc. Eur. Conf. Antennas Propag.*, Apr. 2011, pp. 1531–1535.
- [32] M.-L. Hsu et al., "Bee searching radar with high transmit–receive isolation using pulse pseudorandom code," *IEEE Trans. Microw. Theory Techn.*, vol. 64, no. 12, pp. 4324–4335, Dec. 2016.
- [33] D. E. Root, J. Verspecht, J. Horn and M. Marcu, X-Parameters: Characterization Modeling and Design of Nonlinear RF and Microwave Components. Cambridge, U.K.: Cambridge Univ. Press, 2013.
- [34] Y. Yang, J. Yi, B. Kim, Y. Kim, and M. Park, "Measurement and modeling of two tone transfer characteristics of high power amplifiers," in *Proc. 30th Eur. Microw. Conf.*, Oct. 2000, pp. 1–4.
- [35] C. Li, Modern Radar Circuits and Systems: Radar Equations, document ECE5332, (Class Handout), Texas Tech Univ., Lubbock, TX, USA, 2019
- [36] A. S. M. Miacci and C. M. Rezende, "Basics on radar cross section reduction measurements of simple and complex targets using microwave absorbers," in *Applied Measurement Systems*. Rijeka, Croatia: InTech, 2012



Ashish Mishra (Student Member, IEEE) received the B.E. degree in electronics and telecommunication engineering from the University of Mumbai and the M.S. and Ph.D. degrees in electrical engineering from Texas Tech University, Lubbock, TX, USA, in 2016 and December 2020, respectively.

From February 2020 to August 2020, he was working as an Intern at Unknot.ID, in utilizing mobile phones as sonar devices for human vital signs and gesture monitoring.

From December 2020 to May 2021, he was working as a Postdoctoral Research Associate with Northeastern University. He is currently working at Oculii Corporation. His current research interests include microwave circuits, wireless RF sensors, and their biomedical applications. He was a Reviewer for *Nature* (Springer), IEEE TRANSACTIONS ON MICROWAVE THEORY AND TECHNIQUES, and IEEE ACCESS.



Jing Wang (Student Member, IEEE) received the B.S. degree in communication engineering from the Fujian University of Technology, Fuzhou, China, in 2015, and the Ph.D. degree in electrical engineering from Texas Tech University, Lubbock, TX, USA, in May 2021.

Her current research interests include microwave circuits, wireless RF sensors, and their biomedical applications. She was a recipient of the CH Foundation Graduate Fellowship Award, the IEEE MTT-S IMS

Adaptive Relay Transceiver Design Competition First Place Winner Award, and the IEEE MTT-S IMS High-Sensitivity Motion Radar Design Competition Second Place Winner Award.

all disciplines) in 2019. He received the IEEE MTT-S Graduate Fellowship Award in 2020, the IEEE Microwave Theory and Techniques Society First and Second Place Winner Award in the 2019 Adaptive Relay Transceiver and High-Sensitivity Motion Radar Student Design Competitions, the JT and Margaret Talkington Graduate Fellowship in 2017, and the University of Puerto Rico Honor Tuition Exemption in Fall 2016 and Spring 2017. He is an Active Reviewer of the IEEE TRANSACTIONS ON MICROWAVE THEORY AND TECHNIQUES, the IEEE JOURNAL OF ELECTROMAGNETICS, RF AND MICROWAVES IN MEDICINE AND BIOLOGY, and the IEEE SENSORS JOURNAL.



Daniel Rodriguez (Graduate Student Member, IEEE) received the B.S. degree in electronics and telecommunication engineering from the Universidad Autónoma del Caribe, Barranquilla, Colombia, in 2014, and the M.S. degree from the University of Puerto Rico, Mayagüez, PR, USA, in 2018. He is currently pursuing the Ph.D. degree in electrical engineering with Texas Tech University, Lubbock, TX, USA.

From 2013 to 2014, he worked with the School of Military Engineers, Bogota, Colombia,

in seismic prospection systems for buried explosive artifact detection. He served as an instructor during his time at this institution. His research interests include analog circuits, microwave circuits and systems, wireless sensors, and on chip solar energy harvesting. During Fall 2020, he was with Abbott Laboratories, Sylmar, CA, USA, where he was involved in microwave circuits and systems design for implantable cardiac devices. He was awarded as an HSF Scholar (one of approximately 10 000 of the best and brightest Hispanic students in the country among



Changzhi Li (Senior Member, IEEE) received the B.S. degree in electrical engineering from Zhejiang University, China, in 2004, and the Ph.D. degree in electrical engineering from the University of Florida, Gainesville, FL, USA, in 2009.

He is a Professor with Texas Tech University. His research interests are microwave/millimeterwave sensing for healthcare, security, energy efficiency, structural monitoring, and human-machine interface. He was a

recipient of the IEEE Microwave Theory and Techniques Society (MTT-S) Outstanding Young Engineer Award, the IEEE Sensors Council Early Career Technical Achievement Award, the ASEE Frederick Emmons Terman Award, the IEEE-HKN Outstanding Young Professional Award, the NSF Faculty Early CAREER Award, and the IEEE MTT-S Graduate Fellowship Award. He is an Associate Editor of the IEEE TRANSACTIONS ON MICROWAVE THEORY AND TECHNIQUES and the IEEE JOURNAL OF ELECTROMAGNETICS, RF AND MICROWAVES IN MEDICINE AND BIOLOGY.